ELSEVIER

Chemical Engineering Journal 87 (2002) 339–350

Chemical Engineering Journal

www.elsevier.com/locate/cej

Solutions for the internal boundary layer equations in simultaneously developing flow of power-law fluids within parallel plates channels

R.N.O. Magno, E.N. Macêdo, J.N.N. Quaresma*

Chemical Engineering Department—CT, Universidade Federal do Pará—UFPA, Campus Universitário do Guamá, Rua Augusto Corrêa, 01, 66075-900 Belém, PA, Brazil

Received 13 April 2000; received in revised form 28 November 2001; accepted 28 November 2001

Abstract

The generalized integral transform technique (GITT) is employed in the solution of the boundary layer equations in simultaneously developing laminar flow of power-law non-Newtonian fluids within a parallel plates channel. In the modeling of the related momentum and energy equations within the range of validity of the boundary layer equations, a streamfunction formulation is employed which offers a better computational performance than the primitive-variables formulation. Numerical results for the bulk temperature and Nusselt numbers are established at different axial positions along the channel and for various power-law indices, and critical comparisons with previously reported works in the literature are also performed.

Keywords: Integral transform; Power-law fluids; Simultaneously developing laminar flow; Streamfunction formulation

1. Introduction

The analysis of problems involving heat and fluid flow of non-Newtonian fluids within channels has motivated researchers in many branches of engineering, due to the frequent occurrence of such fluids in different industrial applications. Among them can be pointed out the processing of juices, nectars, jellies and melt cheeses in food industries, applications with polymeric materials in the petrochemical industry, as well as the flow of drilling muds in wells during the drilling operation in the petroleum industry. In such applications, the determination of certain parameters plays an important role in the design and performance improvement of equipment where these fluids are to be processed. Among these parameters, one of the most important is the friction factor, which permits the determination of head losses in channels and ducts. Another important practical quantity is related to the calculation of heat transfer rates, namely, the Nusselt number. The determination of these parameters can be accomplished either experimentally or theoretically, in the latter by solving the appropriate transport equations.

The adequate modeling of the transport phenomena for these fluids, in order to determine the velocity and temperature fields, is when applicable expressed in terms of the so-called boundary layer equations. Despite the great importance in determining the heat and fluid flow characteristics involving non-Newtonian fluids in channels, there are only a few works in the literature dealing with the solution of boundary layer equations in simultaneously developing flow for these fluids, mostly following a power-law model. At this point, we may cite the works by Yau and Tien [1], Lin [2], Lin and Shah [3] and Etemad et al. [4], which have employed purely numerical schemes in the solution of the momentum and energy equations in simultaneously developing flow of power-law fluids inside channels. The excellent review by Hartnett and Kostic [5] has compiled other contributions in the literature for the flow of power-law fluids in rectangular ducts, most of them adopting a conventional finite-difference or finite-element methodology.

On the other hand, a hybrid numerical–analytical approach has been developed for partial differential equations, the well-established generalized integral transform technique (GITT), as reviewed in Refs. [6–8]. This approach is based in eigenfunction expansions yielding solutions with automatic global error control and mild cost increase in multi-dimensional situations. Due to its hybrid nature, this scheme has been well indicated for benchmarking purposes and for the validation of different numerical methods in many classes of problems such as non-linear heat and fluid flow problems, including the Navier–Stokes equations and the laminar and turbulent boundary layer equations in

* Corresponding author.
E-mail address: quaresma@ufpa.br (J.N.N. Quaresma).

1385-8947/02/$ – see front matter
PII: S1385-8947(01)00302-3

Nomenclature

b	half-distance between parallel plates
D_h	hydraulic diameter ($D_h = 4b$)
K	consistency index of the fluid
M_i	normalization integral for the temperature field
n	power-law index
NC	truncation order for the streamfunction field
N_i	normalization integral for the streamfunction field
NM	truncation order for the temperature field
$Nu(x)$	local Nusselt number
$Nu_{av}(x)$	average Nusselt number
Pe	Péclet number
Pr_a	apparent Prandtl number
Pr^+	apparent Prandtl number based on the hydraulic diameter ($Pr^+ = K/(\rho u_0^{1-n} D_h^{n-1}\alpha)$)
p^*	pressure field
p	dimensionless pressure field
Re_a	apparent Reynolds number
Re^+	apparent Reynolds number based on the hydraulic diameter ($Re^+ = \rho u_0^{2-n} D_h^n/K$)
$T(x, y)$	dimensionless temperature distribution
$T^*(x^*, y^*)$	temperature distribution
$\bar{T}_i(x)$	transformed potentials for the temperature field
$T_m(x)$	bulk temperature
T_w	prescribed wall temperature
T_0	inlet temperature
u_0	inlet velocity
u^*, u	longitudinal velocity component, dimensional and dimensionless, respectively
$u_m(x)$	average flow velocity
v^*, v	transversal velocity component, dimensional and dimensionless, respectively
x^*, x	longitudinal coordinate, dimensional and dimensionless, respectively
X_{th}^+	dimensionless longitudinal coordinate defined by Eq. (29)
X^*	dimensionless longitudinal coordinate defined by Eq. (30)
y^*, y	transversal coordinate, dimensional and dimensionless, respectively

Greek letters

α	fluid thermal diffusivity
$\Gamma_i(y)$	eigenfunctions of problem (18)
$\tilde{\Gamma}_i(y)$	normalized eigenfunctions of the temperature field
λ_i	eigenvalues of problem (18)
μ (u_y)	parameter defined by Eq. (5i)
ν	kinematic viscosity
ρ	fluid density
$\Omega_i(y)$	eigenfunctions of problem (17)
$\tilde{\Omega}_i(y)$	normalized eigenfunctions of the streamfunction field
$\phi(x, y)$	filtered potential
$\bar{\phi}_i(x)$	transformed potentials for the streamfunction field
φ_i	eigenvalues of problem (17)
$\psi(x, y)$	streamfunction
$\psi_\infty(y)$	fully developed streamfunction

Subscripts and superscripts

i, j, k	order from eigenvalue problems
$\bar{}$	integral transformed quantities

duct flows as well as convection–diffusion and eigenvalue problems [9–17].

Within this context, the present study aims at solving the boundary layer equations for power-law non-Newtonian fluids in the simultaneously developing laminar flow inside a parallel plates channel, by employing the GITT approach and establishing reliable numerical results for the bulk temperature and Nusselt numbers at the entrance region of the channel.

In the modeling of the problem a formulation in terms of streamfunction is adopted, which has been proved to offer more advantages than the primitive-variables formulation in the GITT solution of the boundary layer equations, demonstrating better convergence behavior and reducing the computational efforts in the calculation of the velocity and temperature fields.

2. Analysis

The problem is geometrically defined by two parallel plates, between which flows a non-Newtonian fluid obeying a power-law model for the shear stress, according to Fig. 1. The main hypotheses for the mathematical formulation of this problem are given as:

– two-dimensional, incompressible and steady-state laminar flow;

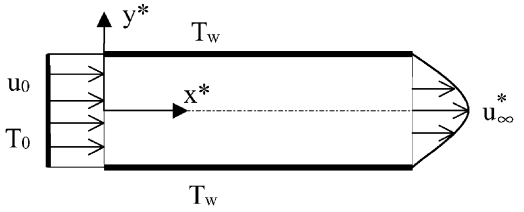

Fig. 1. Geometry and coordinate systems for simultaneously developing duct flow.

– physical properties are taken as constants;
– viscous dissipation and wall conjugation are neglected;
– impermeability and no-slip conditions at the channel walls;
– the inlet velocity and temperature are u_0 and T_0, respectively;
– the channel walls are maintained at an uniform temperature T_w.

With the hypotheses above established, the appropriate equations for the modeling of this problem, the continuity, momentum and energy equations are now simplified. Within the range of validity for the boundary layer hypotheses, this system of equations in dimensionless form can be written as:

$$\frac{\partial u}{\partial x} + \frac{\partial v}{\partial y} = 0, \quad 0 < y < 1,\ x > 0, \tag{1}$$

$$u\frac{\partial u}{\partial x} + v\frac{\partial u}{\partial y} = -\frac{\partial p}{\partial x} + \frac{1}{Re_a}\frac{\partial}{\partial y}\left[\mu(u_y)\frac{\partial u}{\partial y}\right], \quad 0 < y < 1,\ x > 0, \tag{2}$$

$$\frac{\partial p}{\partial y} = 0, \quad 0 < y < 1,\ x > 0, \tag{3}$$

$$u\frac{\partial T}{\partial x} + v\frac{\partial T}{\partial y} = \frac{1}{Pe}\frac{\partial^2 T}{\partial y^2}, \quad 0 < y < 1,\ x > 0, \tag{4}$$

subject to the following inlet and boundary conditions:

$$u(0, y) = 1, \tag{5a}$$

$$T(0, y) = 1, \tag{5b}$$

$$\frac{\partial u(x, 0)}{\partial y} = 0, \tag{5c}$$

$$v(x, 0) = 0, \tag{5d}$$

$$\frac{\partial T(x, 0)}{\partial y} = 0, \tag{5e}$$

$$u(x, 1) = 0, \tag{5f}$$

$$v(x, 1) = 0, \tag{5g}$$

$$T(x, 1) = 0, \tag{5h}$$

where $\mu(u_y)$ is given by:

$$\mu(u_y) = \left[\left(\frac{\partial u}{\partial y}\right)^2\right]^{(n-1)/2}. \tag{5i}$$

The dimensionless groups employed in Eqs. (1)–(5) above are:

$$x = \frac{x^*}{b}, \tag{6a}$$

$$y = \frac{y^*}{b}, \tag{6b}$$

$$u = \frac{u^*}{u_0}, \tag{6c}$$

$$v = \frac{v^*}{u_0}, \tag{6d}$$

$$p = \frac{p^*}{\rho u_0^2}, \tag{6e}$$

$$T = \frac{T^* - T_w}{T_0 - T_w}, \tag{6f}$$

$$Re_a = \frac{\rho u_0^{2-n} b^n}{K}, \tag{6g}$$

$$Pr_a = \frac{K}{\rho u_0^{1-n} b^{n-1} \alpha}, \tag{6h}$$

$$Pe = Re_a Pr_a. \tag{6i}$$

The system of Eqs. (1)–(6) represents the so-called boundary layer equations for a power-law non-Newtonian fluid, and its solution through the GITT approach is the main objective of the present work. In previous works by Machado and Cotta [11], Figueira da Silva [12] and Figueira da Silva and Cotta [13], which dealt with the solution of boundary layer formulation by the same methodology, it was observed that a formulation in terms of streamfunction presents some computational advantages when compared with the primitive-variables formulation. Then, a streamfunction is defined as:

$$\frac{\partial \psi}{\partial y} = u, \tag{7a}$$

$$\frac{\partial \psi}{\partial x} = -v. \tag{7b}$$

Then the vorticity transport and energy equations in the streamfunction-only formulation are written in dimensionless form respectively as:

$$\frac{\partial \psi}{\partial y}\frac{\partial^3 \psi}{\partial x \partial y^2} - \frac{\partial \psi}{\partial x}\frac{\partial^3 \psi}{\partial y^3} = \frac{1}{Re_a}\frac{\partial^2}{\partial y^2}\left[\mu(\psi_{yy})\frac{\partial^2 \psi}{\partial y^2}\right], \quad 0 < y < 1,\ x > 0, \tag{8}$$

$$\frac{\partial \psi}{\partial y}\frac{\partial T}{\partial x} - \frac{\partial \psi}{\partial x}\frac{\partial T}{\partial y} = \frac{1}{Pe}\frac{\partial^2 T}{\partial y^2}, \quad 0 < y < 1,\ x > 0, \tag{9}$$

and the following inlet and boundary conditions:

$$\psi(0, y) = y, \tag{10a}$$

$$T(0, y) = 1, \tag{10b}$$

$$\psi(x, 0) = 0, \tag{10c}$$

$$\frac{\partial^2 \psi(x, 0)}{\partial y^2} = 0, \tag{10d}$$

$$\frac{\partial T(x, 0)}{\partial y} = 0, \tag{10e}$$

$$\psi(x, 1) = 1, \tag{10f}$$

$$\frac{\partial \psi(x, 1)}{\partial y} = 0, \tag{10g}$$

$$T(x,1)=0. \tag{10h}$$

The non-linear coefficient, $\mu(\psi_{yy})$, in the diffusive operator of Eq. (8) is written from Eq. (5i) as

$$\mu(\psi_{yy})=\left[\left(\frac{\partial^2\psi}{\partial y^2}\right)^2\right]^{(n-1)/2}. \tag{11}$$

Following the ideas in the GITT [6,10,12,13,17], in order to select the appropriate auxiliary eigenvalue problem, which shall provide the basis for the eigenfunction expansion, the original problem is made homogeneous in the boundary conditions in the *y*-coordinate, to be eliminated in the integral transformation process. Therefore, the streamfunction is rewritten as:

$$\psi(x,y)=\psi_\infty(y)+\phi(x,y), \tag{12}$$

where $\psi_\infty(y)$ represents the fully developed flow streamfunction, which for a power-law fluid may be obtained as:

$$\psi_\infty(y)=\frac{2n+1}{n+1}y-\frac{n}{n+1}y^{2n+1/n}. \tag{13}$$

Then, the related problem to the "filtered" potential $\phi(x,y)$ and the temperature field after substituting Eq. (12) into Eqs. (8)–(10), becomes

$$\left[\frac{\mathrm{d}\psi_\infty}{\mathrm{d}y}\frac{\partial^3\phi}{\partial x\partial y^2}+\frac{\partial\phi}{\partial y}\frac{\partial^3\phi}{\partial x\partial y^2}\right]-\left[\frac{\mathrm{d}^3\psi_\infty}{\mathrm{d}y^3}\frac{\partial\phi}{\partial x}+\frac{\partial\phi}{\partial x}\frac{\partial^3\phi}{\partial y^3}\right]=\frac{1}{Re_a}\frac{\partial^2}{\partial y^2}\left[\mu(\phi_{yy},\psi''_\infty)\left(\frac{\partial^2\phi}{\partial y^2}+\frac{\mathrm{d}^2\psi_\infty}{\mathrm{d}y^2}\right)\right],\quad 0<y<1,\ x>0, \tag{14}$$

$$\left[\frac{\mathrm{d}\psi_\infty}{\mathrm{d}y}+\frac{\partial\phi}{\partial y}\right]\frac{\partial T}{\partial x}-\frac{\partial\phi}{\partial x}\frac{\partial T}{\partial y}=\frac{1}{Pe}\frac{\partial^2 T}{\partial y^2},\quad 0<y<1,\ x>0, \tag{15}$$

with the following inlet and boundary conditions:

$$\phi(0,y)=y-\psi_\infty(y), \tag{16a}$$

$$T(0,y)=1, \tag{16b}$$

$$\phi(x,0)=0, \tag{16c}$$

$$\frac{\partial^2\phi(x,0)}{\partial y^2}=0, \tag{16d}$$

$$\frac{\partial T(x,0)}{\partial y}=0, \tag{16e}$$

$$\phi(x,1)=0, \tag{16f}$$

$$\frac{\partial\phi(x,1)}{\partial y}=0, \tag{16g}$$

$$T(x,1)=0, \tag{16h}$$

where

$$\mu(\phi_{yy},\psi''_\infty)=\left[\left(\frac{\partial^2\phi}{\partial y^2}+\frac{\mathrm{d}^2\psi_\infty}{\mathrm{d}y^2}\right)^2\right]^{(n-1)/2}. \tag{16i}$$

For the solution of problem (14), by using the GITT, the appropriate eigenvalue problem is taken as:

$$\frac{\mathrm{d}^4\Omega_i(y)}{\mathrm{d}y^4}=\varphi_i^4\Omega_i(y),\quad i=1,2,3,\ldots \tag{17a}$$

$$\Omega_i(0)=0, \tag{17b}$$

$$\frac{\mathrm{d}^2\Omega_i(0)}{\mathrm{d}y^2}=0, \tag{17c}$$

$$\Omega_i(1)=0, \tag{17d}$$

$$\frac{\mathrm{d}\Omega_i(1)}{\mathrm{d}y}=0, \tag{17e}$$

while for the integral transformation of the energy equation, the eigenvalue problem is taken as:

$$\frac{\mathrm{d}^2\Gamma_i(y)}{\mathrm{d}y^2}+\lambda_i^2\Gamma_i(y)=0,\quad i=1,2,3,\ldots \tag{18a}$$

$$\frac{\mathrm{d}\Gamma_i(0)}{\mathrm{d}y}=0, \tag{18b}$$

$$\Gamma_i(1)=0. \tag{18c}$$

Problem (17) can be solved analytically to yield the normalized eigenfunction:

$$\Omega_i(y)=\frac{\sin(\varphi_i y)}{\sin(\varphi_i)}-\frac{\sinh(\varphi_i y)}{\sinh(\varphi_i)},\quad i=1,2,3,\ldots \tag{19a}$$

while the eigenvalues φ_i's are obtained from the transcendental equation:

$$\tanh(\varphi_i)=\tan(\varphi_i),\quad i=1,2,3,\ldots \tag{19b}$$

and the eigenfunction $\Omega_i(y)$'s, can be shown to enjoy the following orthogonality property:

$$\int_0^1\tilde{\Omega}_i(y)\tilde{\Omega}_j(y)\,\mathrm{d}y=\delta_{ij}=\begin{cases}0, & i\neq j\\ 1, & i=j\end{cases}, \tag{19c}$$

$$\tilde{\Omega}_i(y)=\frac{\Omega_i(y)}{N_i^{1/2}}, \tag{19d}$$

$$N_i=1. \tag{19e}$$

Problem (18) can also be solved analytically to yield:

$$\Gamma_i(y)=\cos(\lambda_i y), \tag{20a}$$

$$\lambda_i=(2i-1)\frac{\pi}{2}, \tag{20b}$$

$$\int_0^1\tilde{\Gamma}_i(y)\tilde{\Gamma}_j(y)\,\mathrm{d}y=\delta_{ij}=\begin{cases}0, & i\neq j\\ 1, & i=j\end{cases}, \tag{20c}$$

$$\tilde{\Gamma}_i(y)=\frac{\Gamma_i(y)}{M_i^{1/2}}, \tag{20d}$$

$$M_i=\tfrac{1}{2}. \tag{20e}$$

Properties above allow definition of the integral transform pairs for the streamfunction and temperature fields, respectively, as:

$$\bar{\phi}_i(x) = \int_0^1 \tilde{\Omega}_i(y)\phi(x,y)\,\mathrm{d}y, \quad \text{transform}, \tag{21a}$$

$$\phi(x,y) = \sum_{i=1}^{\infty} \tilde{\Omega}_i(y)\bar{\phi}_i(x), \quad \text{inverse}, \tag{21b}$$

and

$$\bar{T}_i(x) = \int_0^1 \tilde{\Gamma}_i(y)T(x,y)\,\mathrm{d}y, \quad \text{transform}, \tag{21c}$$

$$T(x,y) = \sum_{i=1}^{\infty} \tilde{\Gamma}_i(y)\bar{T}_i(x), \quad \text{inverse}. \tag{21d}$$

To obtain the resulting system of equations for the transformed potentials, the partial differential equations (14) and (15) are integral transformed through the operators $\int_0^1 \tilde{\Omega}_i(y)\,\mathrm{d}y$ and $\int_0^1 \tilde{\Gamma}_i(y)\,\mathrm{d}y$, respectively, leading to the following coupled infinite system of first order non-linear ordinary differential equations:

$$\sum_{j=1}^{\infty} \bar{A}_{ij}\frac{\mathrm{d}\bar{\phi}_j(x)}{\mathrm{d}x} = \bar{D}_i, \quad i = 1,2,3,\ldots \tag{22a}$$

$$\sum_{j=1}^{\infty} \bar{B}_{ij}\frac{\mathrm{d}\bar{\phi}_j(x)}{\mathrm{d}x} + \sum_{j=1}^{\infty} \bar{C}_{ij}\frac{\mathrm{d}\bar{T}_j(x)}{\mathrm{d}x} = \bar{E}_i, \quad i = 1,2,3,\ldots \tag{22b}$$

where

$$\bar{A}_{ij} = (A_{ij\infty} - B_{ij\infty}) + \sum_{k=1}^{\infty}(C_{ijk} - D_{ijk})\bar{\phi}_k(x), \tag{23a}$$

$$\bar{B}_{ij} = -\sum_{k=1}^{\infty} E_{ijk}\bar{T}_k(x), \tag{23b}$$

$$\bar{C}_{ij} = F_{ij\infty} + \sum_{k=1}^{\infty} G_{ijk}\bar{\phi}_k(x), \tag{23c}$$

$$\bar{D}_i = \frac{1}{Re_\mathrm{a}}\int_0^1 \tilde{\Omega}_i''(y)\mu(\phi_{yy}, \psi_\infty'')\left(\frac{\partial^2\phi}{\partial y^2} + \frac{\mathrm{d}^2\psi_\infty}{\mathrm{d}y^2}\right)\mathrm{d}y, \tag{23d}$$

$$\bar{E}_i = -\frac{\lambda_i^2\bar{T}_i(x)}{Pe}, \tag{23e}$$

$$A_{ij\infty} = \int_0^1 \tilde{\Omega}_i(y)\tilde{\Omega}_j''(y)\psi_\infty'(y)\,\mathrm{d}y, \tag{23f}$$

$$B_{ij\infty} = \int_0^1 \tilde{\Omega}_i(y)\tilde{\Omega}_j(y)\psi_\infty'''(y)\,\mathrm{d}y, \tag{23g}$$

$$C_{ijk} = \int_0^1 \tilde{\Omega}_i(y)\tilde{\Omega}_j''(y)\tilde{\Omega}_k'(y)\,\mathrm{d}y, \tag{23h}$$

$$D_{ijk} = \int_0^1 \tilde{\Omega}_i(y)\tilde{\Omega}_j(y)\tilde{\Omega}_k'''(y)\,\mathrm{d}y, \tag{23i}$$

$$E_{ijk} = \int_0^1 \tilde{\Gamma}_i(y)\tilde{\Omega}_j(y)\tilde{\Gamma}_k'(y)\,\mathrm{d}y, \tag{23j}$$

$$F_{ij\infty} = \int_0^1 \tilde{\Gamma}_i(y)\tilde{\Gamma}_j(y)\psi_\infty'(y)\,\mathrm{d}y, \tag{23k}$$

$$G_{ijk} = \int_0^1 \tilde{\Gamma}_i(y)\tilde{\Gamma}_j(y)\tilde{\Omega}_k'(y)\,\mathrm{d}y. \tag{23l}$$

Integral transformation of the inlet conditions (16a) and (16b) yields the following initial conditions for systems (22):

$$\bar{\phi}_i(0) = \int_0^1 \tilde{\Omega}_i(y)(y - \psi_\infty(y))\,\mathrm{d}y = \bar{f}_i, \tag{24a}$$

$$\bar{T}_i(0) = \int_0^1 \tilde{\Gamma}_i(y)\,\mathrm{d}y = \bar{g}_i. \tag{24b}$$

Once systems (22) are solved for the transformed potentials, as discussed bellow, the inversion formulae, Eqs. (21b) and (21d), are recalled to provide the streamfunction and temperature fields, as well as, through differentiation of Eqs. (7a) and (7b), the eigenfunctions expansions for the velocity components:

$$u(x,y) = \psi_\infty'(y) + \sum_{i=1}^{\infty}\tilde{\Omega}_i'(y)\bar{\phi}_i(x), \tag{25a}$$

$$v(x,y) = -\sum_{i=1}^{\infty}\tilde{\Omega}_i(y)\frac{\mathrm{d}\bar{\phi}_i(x)}{\mathrm{d}x}. \tag{25b}$$

The local and average Nusselt numbers are defined, respectively, as:

$$Nu(x) = -\frac{4}{T_\mathrm{m}(x)}\frac{\partial T(x,1)}{\partial y}, \tag{26a}$$

$$Nu_\mathrm{av}(x) = \frac{1}{x}\int_0^x Nu(x')\,\mathrm{d}x', \tag{26b}$$

or by integrating Eq. (26a),

$$Nu_\mathrm{av}(x) = -\frac{4Pe}{x}\ln[T_\mathrm{m}(x)], \tag{26c}$$

where

$$T_\mathrm{m}(x) = \frac{\int_0^1 u(x,y)T(x,y)\,\mathrm{d}y}{u_\mathrm{m}(x)}. \tag{26d}$$

Through application of the inversion formulae given by Eqs. (21b) and (21d), and by considering that $u_\mathrm{m}(x) = 1$, Eq. (26d) becomes

$$T_\mathrm{m}(x) = \sum_{i=1}^{\infty}\left[H_{i\infty} + \sum_{j=1}^{\infty} I_{ij}\bar{\phi}_j(x)\right]\bar{T}_i(x), \tag{26e}$$

$$H_{i\infty} = \int_0^1 \tilde{\Gamma}_i(y)\psi'_\infty(y)\,\mathrm{d}y, \tag{26f}$$

$$I_{ij} = \int_0^1 \tilde{\Gamma}_i(y)\tilde{\Omega}'_j(y)\,\mathrm{d}y. \tag{26g}$$

Systems (22a) and (22b) constitute a non-linear initial value problem of infinite equations, which have to be truncated in sufficiently high orders, such as NC and NM, in order to calculate the transformed potentials for the streamfunction and temperature fields, $\bar{\phi}_i(x)$ and $\bar{T}_i(x)$, respectively. From a computational point of view, it is more appropriate that both systems are solved simultaneously along the entrance region. In the solution of such systems, due to their stiff characteristics, appropriate subroutines have to be employed, such as the subroutine DIVPAG from the IMSL Library [18]. This subroutine provides the important feature of automatic error control over the solution of the ordinary differential equations system, allowing the user to establish error targets for the transformed potentials, a priori. A straightforward way to organize systems (22), so as to permit their simultaneous solution, is to combine their truncated versions in only one system of ordinary differential equations, such as:

$$E(Y)\frac{\mathrm{d}Y}{\mathrm{d}x} = D(Y). \tag{27}$$

In the vector Y, of the transformed potentials, which has dimension (NC + NM), the NC first positions are occupied by $\bar{\phi}_i$ ($i = 1, 2, \ldots, \mathrm{NC}$), and the remaining positions by $\bar{T}_i$ ($i = 1, 2, \ldots, \mathrm{NM}$), the vector D has dimension (NC + NM), and the matrix E has dimension (NC + NM) × (NC + NM). The system (27) is better envisioned when written in the matrix form as:

$$\begin{bmatrix} & 0 & \cdots & 0 \\ \bar{A}_{ij}(\bar{\phi}) & \vdots & \ddots & \vdots \\ & 0 & \cdots & 0 \\ \bar{B}_{\mathrm{ij}}(\bar{T}) & & \bar{C}_{ij}(\bar{\phi}) & \end{bmatrix} \begin{bmatrix} \dfrac{\mathrm{d}\bar{\phi}_j}{\mathrm{d}x} \\ \dfrac{\mathrm{d}\bar{T}_j}{\mathrm{d}x} \end{bmatrix} = \begin{bmatrix} \bar{D}_i(\bar{\phi}) \\ \bar{E}_i(\bar{T}) \end{bmatrix}. \tag{28}$$

Since the transformed potentials are calculated within a prescribed accuracy, the global errors in the streamfunction and temperature fields are finally controlled by the truncation orders (NC and NM) for system (28), as the eigenfunction expansion, Eqs. (21b) and (21d), converge within the requested accuracy at selected domain positions.

3. Results and discussion

The momentum equation in terms of the streamfunction formulation and the energy equation were simultaneously solved under controlled accuracy and, numerical results were produced for different power-law indices and apparent Prandtl numbers along the entrance of the channel. For all computations equal truncation orders NC = NM were adopted in the solution of system (28) through the subroutine DIVPAG (IMSL Library [18]) with a relative error target of 10^{-8}. For this purpose, a computational code was developed in FORTRAN 90 programming language and implemented on a PENTIUM-II 400 MHz computer. Aspects on the results of the velocity field were previously discussed in a paper by Magno et al. [19].

Results were obtained as functions of the following dimensionless axial coordinates X^+_{th} and X^* as defined below, respectively,

$$X^+_{\mathrm{th}} = \frac{x^*}{D_{\mathrm{h}}Re^+Pr^+}, \tag{29}$$

$$X^* = \frac{x^*}{bRe_{\mathrm{a}}}. \tag{30}$$

For both cases, the apparent Reynolds numbers, Re_{a} and Re^+, were taken equal to 2000 (except when indicate in the titles of the tables), since these dimensionless axial coordinates are independent of these parameters.

First, in Table 1 is illustrated the convergence behavior on the bulk temperature for $Pr_{\mathrm{a}} = 0.72$ and $n = 1$ along the channel length, as well as a comparison with those results presented by Figueira da Silva [12] and Figueira da Silva and Cotta [13], in order to validate the numerical code developed

Table 1
Convergence behavior on the bulk temperature for $Pr_{\mathrm{a}} = 0.72$ and $n = 1$ along the channel length

$X^+_{\mathrm{th}} \times 10^3$	NC = NM						Refs. [12,13]
	20	40	60	80	100	120	
0.0434	0.98077	0.98081	0.98089	0.98095	0.98100	0.98104	0.98089
0.2600	0.95179	0.95222	0.95241	0.95251	0.95257	0.95261	0.95240
0.6080	0.92510	0.92563	0.92582	0.92591	0.92597	0.92601	0.92581
1.3000	0.88802	0.88857	0.88875	0.88884	0.88889	0.88892	0.88874
2.6000	0.83701	0.83752	0.83768	0.83776	0.83780	0.83783	0.83768
4.3400	0.78354	0.78400	0.78415	0.78422	0.78425	0.78428	0.78414
8.6800	0.67918	0.67957	0.67968	0.67974	0.67977	0.67979	0.67968
23.4000	0.43434	0.43458	0.43465	0.43469	0.43471	0.43472	0.43466
43.4000	0.23761	0.23774	0.23778	0.23780	0.23781	0.23781	0.23779
94.2000	0.051334	0.051362	0.051371	0.051375	0.051377	0.051379	0.05138

Table 2
Convergence behavior on the bulk temperature for $Pr_a = 50$ and $n = 1$ along the channel length

$X_{th}^+ \times 10^3$	NC = NM					
	20	40	60	80	100	120
0.0075	0.99554	0.99620	0.99620	0.99614	0.99609	0.99604
0.0200	0.99321	0.99344	0.99331	0.99320	0.99313	0.99308
0.0563	0.98811	0.98788	0.98768	0.98756	0.98749	0.98745
0.1190	0.98136	0.98094	0.98074	0.98063	0.98057	0.98053
0.2750	0.96851	0.96804	0.96786	0.96777	0.96771	0.96768
0.5250	0.95228	0.95184	0.95168	0.95160	0.95156	0.95153
0.9380	0.93037	0.92998	0.92985	0.92978	0.92975	0.92972
1.5600	0.90290	0.90257	0.90246	0.90240	0.90237	0.90235
3.1300	0.84697	0.84671	0.84662	0.84658	0.84656	0.84654
6.8800	0.74461	0.74442	0.74436	0.74432	0.74431	0.74429

here and to demonstrate that consistent results were computed. From this table can be verified an excellent convergence rate of the results and, with a truncation order within the range of 20–40 terms in the summations, a convergence of two digits is reached and, in the range of 100–120 terms at least four significant digits are fully converged in the bulk temperature. A similar analysis along the channel length is illustrated in Table 2 for the case of $Pr_a = 50$ and $n = 1$. From this table an excellent convergence rate of the results can also be verified.

After the convergence analysis on the bulk temperature is made, Table 3 brings comparisons of the present average Nusselt numbers with those obtained by Figueira da Silva [12], Figueira da Silva and Cotta [13] and Hwang and Fan [20], as presented by Shah and London [21], for the cases of $n = 1$ and $Pr_a = 0.72$ and 50 at various axial positions. In both cases analyzed, a truncation order of NC = NM = 120 was employed in the summations. The slight discrepancy among the present results with those in the works of Figueira da Silva [12] and Figueira da Silva and Cotta [13], which also utilized the GITT approach for the solution of the same problem, can be explained by the fact that their results were calculated with a relative error target of 10^{-6} and a truncation order of NC = NM = 80. The more evident difference with those results by a finite-difference scheme in the work by Hwang and Fan [20] may be due to the fact that the Nusselt number calculated in Ref. [20] was obtained from the derivative of the fluid temperature at the duct wall that is a more difficult task for the finite differences approximation with a regular mesh, specially for lower apparent Prandtl numbers. This difficulty is alleviated in the present methodology, since the temperature field is analytical in the transversal direction, so that the average Nusselt number is calculated through the direct integration of the energy equation.

In addition, comparisons with other previous works are made in Tables 4–6 for different power-law indices and apparent Prandtl numbers, and as can be noted from these tables, the excellent convergence behavior of the results for the local Nusselt number and the good agreement with previous ones also validate the numerical code developed in the present work as well as indicate the consistency of the present results. Also in Fig. 2 is shown a comparison with the works of Quaresma and Macêdo [22] and Cotta and Özisik [23] for the case of $Pr_a \to \infty$, which represents the thermally developing flow situation, and as can be seen the results are in excellent agreement,

Table 3
Comparison of average Nusselt numbers for $n = 1$, $Pr_a = 0.72$ and 50 along the channel length

$Pr_a = 0.72$				$Pr_a = 50$			
$X_{th}^+ \times 10^3$	Present work	Refs. [12,13]	Ref. [20]	$X_{th}^+ \times 10^3$	Present work	Refs. [12,13]	Ref. [20]
0.0434	110.26	111.1	116.1	0.0075	132.23	122.3	150.2
0.0868	78.682	79.24	72.87	0.0138	101.80	96.84	108.4
0.2600	46.684	46.89	44.14	0.0200	86.852	83.68	89.93
0.4340	36.832	36.96	35.09	0.0250	78.967	76.56	80.79
0.6080	31.609	31.70	30.23	0.0563	56.087	55.24	54.95
0.9550	25.872	25.93	24.91	0.0875	46.772	46.30	45.19
1.3000	22.644	22.68	21.90	0.1190	41.309	41.00	39.77
1.7400	20.028	20.06	19.52	0.1500	37.682	37.45	36.20
2.6000	17.014	17.03	16.63	0.2750	29.865	29.76	28.73
3.4700	15.211	15.22	14.90	0.4000	26.045	25.98	25.15
4.3400	13.997	14.01	13.74	0.5250	23.657	23.61	22.91
6.0800	12.440	12.45	12.24	0.6250	22.272	22.24	21.62
8.6800	11.117	11.12	10.96	0.9380	19.421	19.40	18.92
14.800	9.6866	9.689	9.593	1.2500	17.678	17.66	17.26
23.400	8.9002	8.902	8.827	1.5600	16.467	16.46	16.10
32.100	8.5315	8.532	8.474	1.8800	15.528	15.52	15.23
43.400	8.2734	8.274	8.225	3.1300	13.306	13.30	13.11
65.100	8.0292	8.029	7.986	4.3800	12.088	12.09	11.94
94.200	7.8783	7.878	7.792	5.6300	11.295	11.29	11.17
151.90	7.7500	7.749	7.707	6.8800	10.731	10.73	10.63

Table 4
Comparison of local Nusselt numbers for $n = 1$, $Re_a = 250$ and $Pr_a = 5$ along the channel length

X_{th}^+	NC = NM						Campos Silva et al. [15]	Etemad et al. [4]
	10	20	40	60	80	100		
1.25×10^{-4}	27.03	28.10	28.18	28.14	28.11	28.10	27.75	24.72
4.38×10^{-4}	16.98	17.07	17.04	17.03	17.02	17.02	16.80	15.82
7.5×10^{-4}	14.04	14.05	14.03	14.02	14.02	14.02	13.70	13.34
2×10^{-3}	10.36	10.36	10.35	10.35	10.35	10.35	10.10	10.27
6.25×10^{-3}	8.150	8.148	8.147	8.147	8.146	8.146	8.20	8.15
1×10^{-2}	7.728	7.728	7.727	7.727	7.727	7.727	7.79	7.72
1.25×10^{-2}	7.627	7.626	7.626	7.626	7.626	7.626	7.70	7.63
2.5×10^{-2}	7.542	7.542	7.542	7.542	7.542	7.542	7.56	7.55
4.06×10^{-2}	7.541	7.541	7.541	7.541	7.541	7.541	7.54	7.54

Table 5
Comparison of local Nusselt numbers for $n = 0.5$, $Re_a = 250$ and $Pr_a = 0.5$ along the channel length

X_{th}^+	NC = NM						Lin [2]	Etemad et al. [4]
	10	20	40	60	80	100		
6.09×10^{-4}	22.24	20.76	20.47	20.42	20.41	20.41	20.71	20.97
1.102×10^{-3}	16.50	15.89	15.83	15.82	15.81	15.82	16.57	15.98
2.173×10^{-3}	12.25	12.17	12.15	12.15	12.16	12.16	12.29	12.12
4.045×10^{-3}	9.955	9.931	9.931	9.934	9.936	9.938	9.87	9.86
5.712×10^{-3}	9.099	9.088	9.090	9.093	9.094	9.095	9.05	9.03
1.0465×10^{-2}	8.243	8.242	8.243	8.244	8.244	8.244	8.27	8.20
2.0552×10^{-2}	7.992	7.991	7.991	7.991	7.990	7.990	8.00	7.97
2.6533×10^{-2}	7.968	7.967	7.967	7.967	7.967	7.966	7.96	7.95

once again validating the computational code developed here.

Figs. 3 and 4 show the development of the temperature field along the axial coordinate, X^*, for the cases of $Pr_a = 1$ and 50 and by adopting the power-law indices $n = 0.75$, 1 and 3, respectively. From these figures, it is observed that the development of the temperature profiles is more rapidly reached for the case of apparent Prandtl number $Pr_a = 1$, than for the case of $Pr_a = 50$. For the situation of $Pr_a = 1$, the tendency of the temperature profile is to be fully developed in a position closer the channel inlet, such as at positions near to $X^* = 0.8$. It is also verified the strong influence of the power-law index in the vicinities of the channel wall, where for the case of $n = 0.75$ the temperature gradients are more pronounced than for $n = 3$, mainly for the case of apparent Prandtl number $Pr_a = 1$, whereas for $Pr_a = 50$ the results for temperature profiles are practically coincident in almost all positions along the channel length for all power-law indices studied; certainly, this fact will affect the Nusselt numbers in the entrance region.

The analysis of the behavior of the temperature field is now reported in terms of local Nusselt numbers for three different power-law indices, namely $n = 0.75$, 1 and 3, and for the values of apparent Prandtl numbers $Pr_a = 1$

Table 6
Comparison of local Nusselt numbers for $n = 0.5$, $Re_a = 250$ and $Pr_a = 5$ along the channel length

X_{th}^+	NC = NM						Lin [2]	Etemad et al. [4]
	10	20	40	60	80	100		
7.814×10^{-4}	15.11	15.04	15.01	15.01	15.01	15.01	15.21	14.83
9.989×10^{-4}	13.81	13.76	13.74	13.73	13.73	13.74	13.86	13.59
1.2052×10^{-3}	12.93	12.89	12.88	12.88	12.88	12.88	13.29	12.76
1.8029×10^{-3}	11.37	11.35	11.34	11.34	11.34	11.34	11.43	11.28
2.3350×10^{-3}	10.56	10.55	10.55	10.55	10.55	10.55	10.6	10.52
4.0173×10^{-3}	9.289	9.284	9.283	9.283	9.284	9.284	9.29	9.29
6.0257×10^{-3}	8.637	8.635	8.634	8.635	8.635	8.635	8.65	8.64
1.01102×10^{-2}	8.138	8.137	8.137	8.137	8.137	8.137	8.21	8.14
2.05247×10^{-2}	7.948	7.948	7.948	7.948	7.948	7.948	7.94	7.95

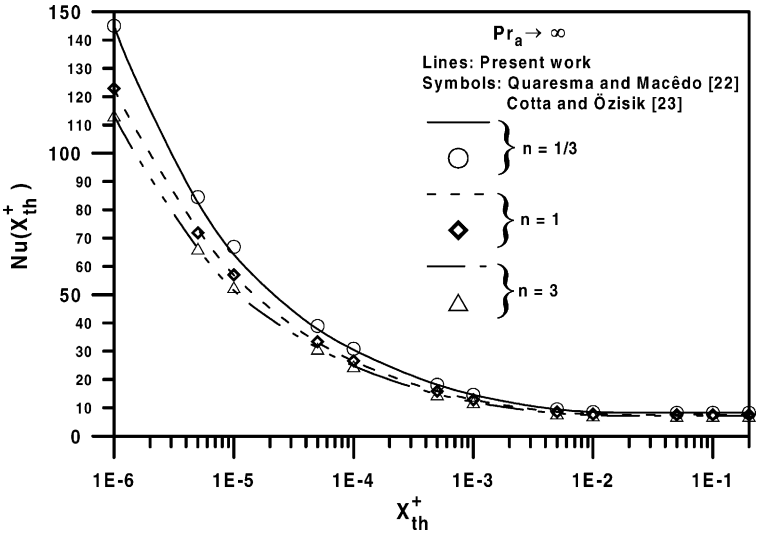

Fig. 2. Comparison of local Nusselt numbers in thermally developing flow.

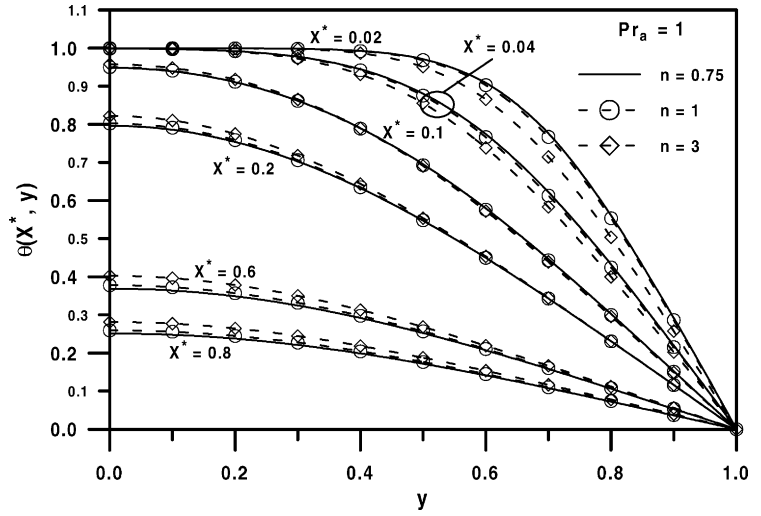

Fig. 3. Development of the temperature field along the channel length for $Pr_a = 1$ and $n = 0.75$, 1 and 3.

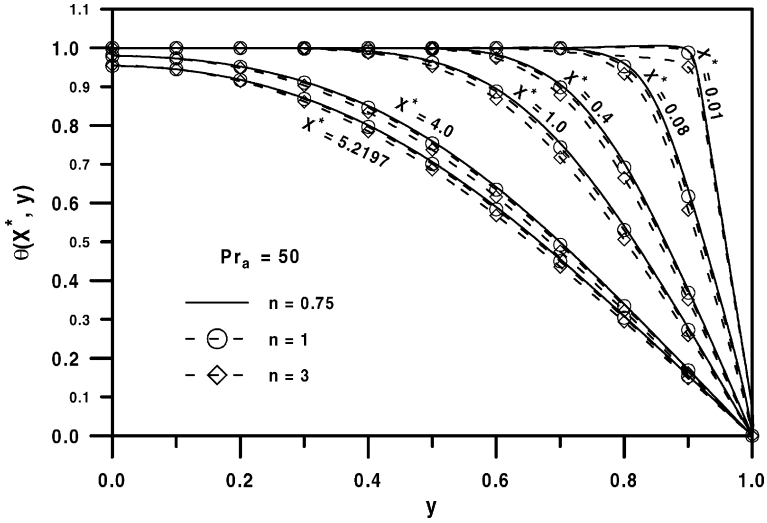

Fig. 4. Development of the temperature field along the channel length for $Pr_a = 50$ and $n = 0.75$, 1 and 3.

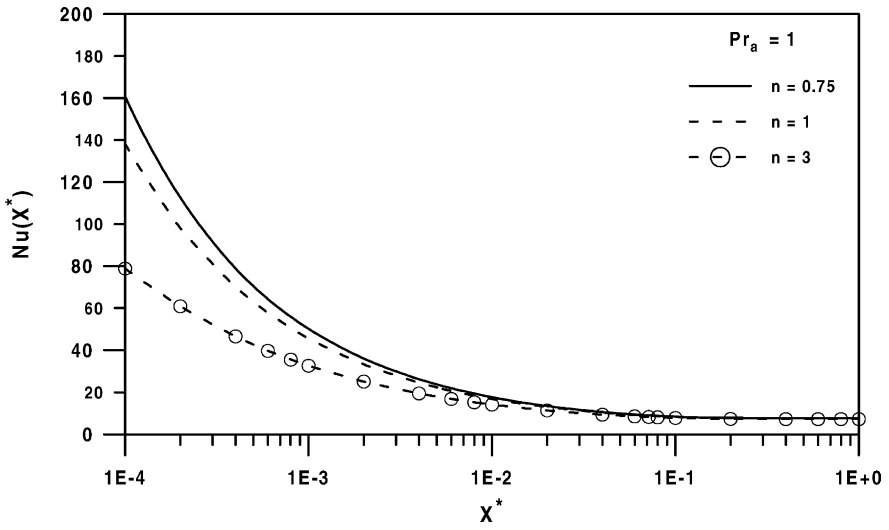

Fig. 5. Local Nusselt numbers in the simultaneously developing region for the case of $Pr_a = 1$ and $n = 0.75$, 1 and 3.

and 50. In Fig. 5 results are presented for the local Nusselt number in the thermal entry region for the case of $Pr_a = 1$ and $n = 0.75$, 1 and 3. From this figure it can be noticed the strong influence of the power-law index in the local Nusselt number behavior. This effect can be explained by the fact that for power-law index greater than unity the convective effects near the wall diminish and consequently the thermal exchange is less intensified resulting in lower values for the Nusselt numbers. Similar observations are verified from Fig. 6, where local Nusselt numbers are presented for the case of $Pr_a = 50$ and $n = 0.75$, 1, and 3. From these figures it can also be noticed the nearly coincident values for the asymptotic Nusselt numbers at different power-law indices, $n = 0.75$, 1 and 3, and for fixed Prandtl numbers.

Finally in Fig. 7, it is shown a comparison among the results for the local Nusselt number, in the simultaneously developing region, for $Pr_a = 1$ and 50 and $n = 0.75$, obtained by the present methodology against those obtained through the numerical scheme employed by Yau and Tien [1]. A marked difference between the two sets of results is verified in positions near the entrance region, which may be due to the numerical scheme adopted by these authors, that certainly affects the final results. The adopted scheme overpredicts the results for the velocity field (Magno et al. [19]), while underpredicting the results for the Nusselt number for $Pr_a = 1$, and in addition showing a cross-over behavior for $Pr_a = 50$, in relation to the present results, as can be observed from Fig. 7.

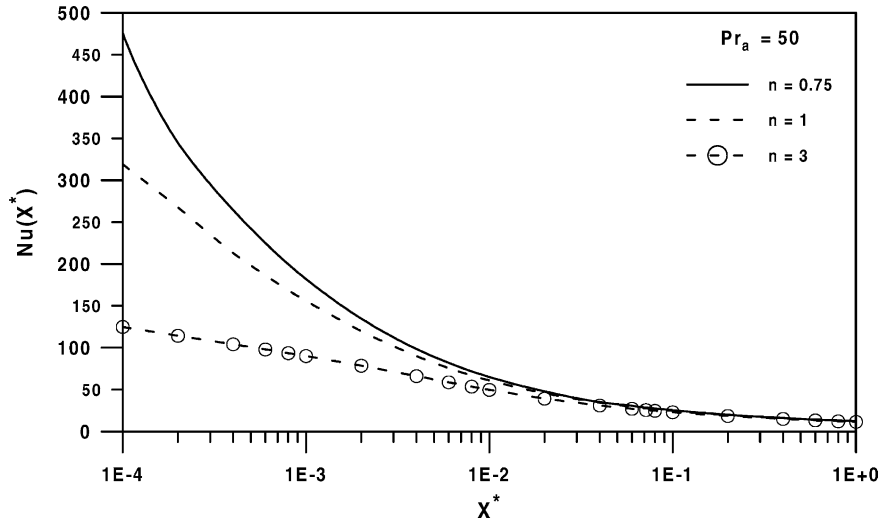

Fig. 6. Local Nusselt numbers in the simultaneously developing region for the case of $Pr_a = 50$ and $n = 0.75$, 1 and 3.

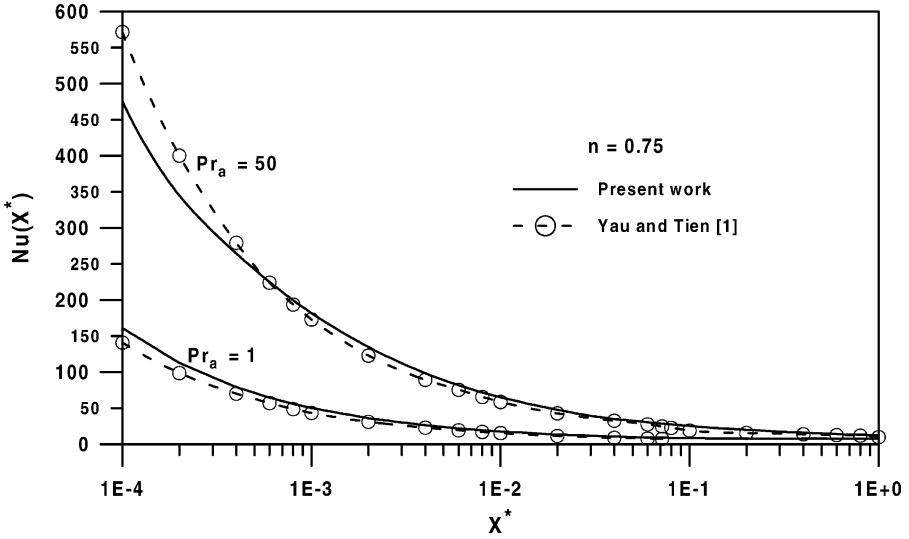

Fig. 7. Comparison of local Nusselt numbers in the simultaneously developing region for $n = 0.75$ and $Pr_a = 1$ and 50.

4. Conclusions

The GITT was successfully employed in the solution of the internal boundary layer equations in the simultaneously developing laminar flow of power-law non-Newtonian fluids. Benchmark results for the temperature field and Nusselt numbers in the entrance region were then tabulated and graphically presented for different power-law indices and apparent Prandtl numbers. It was verified that for values of power-law indices greater than unity, the convective effects near the wall diminish and consequently lower values for the Nusselt numbers in the entrance region are obtained, whereas for the thermally developed region nearly coincident values for the asymptotic Nusselt numbers at different power-law indices, and for fixed Prandtl numbers are computed. Comparisons with previous results in the literature given by Yau and Tien [1] were performed demonstrating that their results for Nusselt numbers are markedly affected by the numerical scheme employed in their work.

References

[1] J. Yau, C. Tien, Simultaneous development of velocity and temperature profiles for laminar flow of a non-Newtonian fluid in the entrance region of flat ducts, Can. J. Chem. Eng. 41 (1963) 139–145.
[2] T. Lin, Numerical solutions of heat transfer to yield power law fluids in the entrance region, M.Sc. Thesis, University of Wisconsin, Milwaukee, WI, 1977.
[3] T. Lin, V.L. Shah, Numerical solution of heat transfer to yield power law fluids flowing in the entrance region, in: Proceedings of the Sixth International Heat Transfer Conference, Vol. 5, Toronto, Canada, 1978, pp. 317–322.
[4] S.Gh. Etemad, A.S. Mujumdar, B. Huang, Viscous dissipation effects in entrance region heat transfer for a power law fluid flowing between parallel plates, Int. J. Heat Fluid Flow 15 (1994) 122–131.
[5] J.P. Hartnett, M. Kostic, Heat transfer to Newtonian and non-Newtonian fluids in rectangular ducts, Adv. Heat Tran. 19 (1989) 247–356.
[6] R.M. Cotta, Integral Transforms in Computational Heat and Fluid Flow, CRC Press, Boca Raton, FL, 1993.
[7] R.M. Cotta, Benchmark results in computational heat and fluid flow: the integral transform method, Int. J. Heat Mass Tran. (Invited Paper) 37 (Suppl. 1) (1994) 381–393.
[8] R.M. Cotta, Simulations and benchmarks in thermal-fluids sciences: the integral transform approach, in: Proceedings of the Third North–Northeastern Congress of Mechanical Engineering, Vol. 2, Belém, Brazil, 1994, p9–p27.
[9] R.M. Cotta, Hybrid numerical analytical approach to nonlinear diffusion problems, Numer. Heat Tran. B 17 (1990) 217–226.
[10] J.S. Pérez Guerrero, R.M. Cotta, Integral transform solution for the lid-driven cavity flow problem in stream-function only formulation, Int. J. Numer. Meth. Fluids 15 (1992) 399–409.
[11] H.A. Machado, R.M. Cotta, Integral transform method for boundary layer equations in simultaneous heat and fluid flow problems, Int. J. Numer. Meth. Heat Fluid Flow 5 (1995) 225–237.
[12] E. Figueira da Silva, Integral transformation of the boundary layer equations for internal convection in the streamfunction and primitive variables formulations, M.Sc. Thesis, Mechanical Engineering Department, Universidade Federal do Rio de Janeiro, Rio de Janeiro, Brazil, 1994 (in Portuguese).
[13] E. Figueira da Silva, R.M. Cotta, Benchmark results for internal forced convection through integral transformation, Int. Commun. Heat Mass Tran. 23 (1996) 1019–1029.
[14] R.M. Cotta, L.C.G. Pimentel, Developing turbulent duct flow: hybrid solution via integral transforms and algebraic model, Int. J. Numer. Meth. Heat Fluid Flow 8 (1998) 10–26.
[15] J.B. Campos Silva, R.M. Cotta, J.B. Aparecido, Analytical solutions to simultaneously developing laminar flow inside parallel-plates channel, Int. J. Heat Mass Tran. 35 (1992) 887–895.
[16] M.D. Mikhailov, R.M. Cotta, Integral transform method for eigenvalue problems, Commun. Numer. Meth. Eng. 10 (1994) 827–835.
[17] J.S. Pérez Guerrero, R.M. Cotta, Integral transform solution of developing laminar duct flow in Navier–Stokes formulation, Int. J. Numer. Meth. Fluids 20 (1995) 1203–1213.
[18] IMSL Library, Math/Lib., Houston, TX, 1991.

[19] R.N.O. Magno, J.N.N. Quaresma, E.N. Macêdo, Integral transform solution for the internal boundary layer of non-Newtonian fluids, Hybrid Meth. Eng. 1 (1999) 173–184.
[20] C.L. Hwang, L.T. Fan, Finite difference analysis of forced-convection heat transfer in entrance region of a flat rectangular duct, Appl. Sci. Res. A 13 (1964) 401–422.
[21] R.K. Shah, A.L. London, Laminar flow forced convection in ducts, Adv. Heat Tran. (Suppl. 1) (1978).
[22] J.N.N. Quaresma, E.N. Macêdo, Integral transform solution for the forced convection of Herschel–Bulkley fluids in circular tubes and parallel-plates ducts, Braz. J. Chem. Eng. 15 (1998) 77–89.
[23] R.M. Cotta, M.N. Özisik, Laminar forced convection of power-law non-Newtonian fluids inside ducts, Wärme-und Stoffübertragung 20 (1986) 211–218.